Bone 175 (2023) 116859

Contents lists available at ScienceDirect

Bone

journal homepage: www.elsevier.com/locate/bone

Full Length Article

The contribution of lower-mineralized tissue to the healing of distal radius fractures assessed using HR-pQCT

Melissa S.A.M. Bevers [a,b,c,1], Frans L. Heyer [b,d,1], Caroline E. Wyers [a,b,e], Bert van Rietbergen [c,f], Piet P.M.M. Geusens [e,g], Heinrich M.J. Janzing [d], Okke Lambers Heerspink [h], Martijn Poeze [b,i], Joop P. van den Bergh [a,b,e,*]

[a] Department of Internal Medicine, VieCuri Medical Center, Venlo, the Netherlands
[b] NUTRIM School for Nutrition and Translational Research In Metabolism, Maastricht University Medical Center, Maastricht, the Netherlands
[c] Department of Biomedical Engineering, Eindhoven University of Technology, Eindhoven, the Netherlands
[d] Department of Surgery, VieCuri Medical Center, Venlo, the Netherlands
[e] Department of Internal Medicine, Subdivision of Rheumatology, Maastricht University Medical Center, Maastricht, the Netherlands
[f] Department of Orthopedic Surgery, Maastricht University Medical Center, Maastricht, the Netherlands
[g] Department of Medicine and Life Sciences, Hasselt University, Belgium
[h] Department of Orthopedic Surgery, VieCuri Medical Center, Venlo, the Netherlands
[i] Department of Surgery and Trauma Surgery, Maastricht University Medical Center, Maastricht, the Netherlands

ARTICLE INFO

Keywords:
Distal radius fracture
Fracture healing
HR-pQCT
Dual-threshold segmentation
micro-finite element analysis
Bone strength

ABSTRACT

High-resolution peripheral quantitative CT (HR-pQCT) enables quantitative assessment of distal radius fracture healing. In previous studies, lower-mineralized tissue formation was observed on HR-pQCT scans, starting early during healing, but the contribution of this tissue to the stiffness of distal radius fractures is unknown. Therefore, the aim of this study was to investigate the contribution of lower-mineralized tissue to the stiffness of fractured distal radii during the first twelve weeks of healing. We did so by combining the results from two series of micro-finite element (μFE-) models obtained using different density thresholds for bone segmentation. Forty-five postmenopausal women with a conservatively-treated distal radius fracture had HR-pQCT scans of their fractured radius at baseline (BL; 1–2 weeks post-fracture), 3–4 weeks, 6–8 weeks, and 12 weeks post-fracture. Compression stiffness (S) was computed using two series of μFE-models from the scans: one series (M_{single}) included only higher-mineralized tissue (>320 mg HA/cm^3), and one series (M_{dual}) differentiated between lower-mineralized tissue (200–320 mg HA/cm^3) and higher-mineralized tissue. μFE-elements were assigned a Young's Modulus of 10 GPa (higher-mineralized tissue) or 5 GPa (lower-mineralized tissue), and an axial compression test to 1 % strain was simulated. The contribution of the lower-mineralized tissue to S was quantified as the ratio S_{dual}/S_{single}. Changes during healing were quantified using linear mixed effects models and expressed as estimated marginal means (EMMs) with 95 %-confidence intervals (95 %-CI). Median time to cast removal was 5.0 (IQR: 1.1) weeks. S_{dual} and S_{single} gradually increased during healing to a significantly higher value than BL at 12 weeks post-fracture (both $p < 0.0001$). In contrast, S_{dual}/S_{single} was significantly higher than BL at 3–4 weeks post-fracture ($p = 0.0010$), remained significantly higher at 6–8 weeks post-fracture ($p < 0.0001$), and then decreased to BL-values at the 12-week visit. EMMs ranged between 1.05 (95 %-CI: 1.04–1.06) and 1.08 (95 %-CI: 1.07–1.10). To conclude, combining stiffness results from two series of μFE-models obtained using single- and dual-threshold segmentation enables quantification of the contribution of lower-mineralized tissue to the stiffness of distal radius fractures during healing. This contribution is minor but changes significantly around the time of cast removal. Its course and timing during healing may be clinically relevant. Quantification of the contribution of lower-mineralized tissue to stiffness gives a more complete impression of strength recovery post-fracture than the evaluation of stiffness using a single series of μFE-models.

* Corresponding author at: Tegelseweg 210, NL – 5912 BL Venlo, the Netherlands.
E-mail address: joop.vandenbergh@maastrichtuniversity.nl (J.P. van den Bergh).
[1] These authors share first authorship.

https://doi.org/10.1016/j.bone.2023.116859
Received 17 May 2023; Received in revised form 3 July 2023; Accepted 25 July 2023
Available online 26 July 2023

1. Introduction

Distal radius fractures are among the most common fractures in elderly [1,2], but assessment of the healing and union of these fractures is complex. In older individuals, they comprise nearly 20 % of all fractures [1]. Their prevalence is increasing, among others due to the aging population and an increased physical activity among elderly [3]. The majority of distal radius fractures in elderly are treated conservatively using cast immobilization [4]. Dutch guidelines prescribe to consider cast treatment for 3–5 weeks depending on fracture displacement and reduction [5]. However, evidence for the optimal immobilization period is limited, especially for reduced fractures [5–8]. The development of evidence-based guidelines is furthermore challenging due to a lack of consensus on and subjectivity of assessing distal radius fracture healing and union [9], which is a problem for fractures in general [10,11]. The assessment of fracture union in clinical practice often includes a physical and radiographic examination [9–11]. Factors, such as biological and biomechanical ones, are not standardly evaluated in clinical practice, but they are essential in fracture healing [12,13]. Such factors could be clinically valuable when they capture changes during the healing process that provide insights into whether a fracture can be clinically considered as healed (*i.e.* when a fracture is able to resist the loading that is associated with daily activities).

High-resolution peripheral quantitative CT (HR-pQCT) enables detailed assessment of changes during fracture healing [14–19]. In conservatively-treated distal radius fractures in postmenopausal women, large visual changes around the fracture region have been observed on HR-pQCT scans early during healing [15]. Specifically, trabeculae became 'blurred' and thereby less well distinguishable from three to four weeks post-fracture and were re-distinguishable again later during healing [15]. These changes were suggested to reflect the formation and concomitant and subsequent remodeling of woven bone, known phases in fracture healing that are important in the stabilization of a fracture and the formation of new bone [20–22]. In the same studies, the stiffness of the fractured radii, computed using micro-finite element (μFE-) analysis, increased significantly compared to baseline later during healing and continued to increase months after cast removal [15,16]. The early lower-mineralized tissue is not standardly included in μFE-models from HR-pQCT scans to compute stiffness, and available HR-pQCT data are inconclusive about the differences in the computed stiffness of distal radius fractures during healing between μFE-models that include lower-mineralized tissue and standard μFE-models that do not include this tissue [15,18]. Consequently, the contribution of the lower-mineralized tissue to fracture stiffness is unknown. Recently, multiple density thresholds between 200 and 680 mg HA/cm^3 were used for trabecular bone in an HR-pQCT study on local bone remodeling during distal radius fracture healing to evaluate trabecular bone around the fracture region with densities lower and higher than normally evaluated in HR-pQCT analyses (>320 mg HA/cm^3) [17]. Application of such method to generate multiple series of μFE-models that include tissue of different densities may enable study of the contribution of lower-mineralized tissue to fracture stiffness.

The reported differences between the timing of cast removal and the changes in computed stiffness suggest a difference between the clinical and biomechanical perspective of a healed fracture [15,16]. Possibly, the lower-mineralized tissue could contribute to explaining this difference and play a role in the biomechanical recovery of distal radius fractures early during healing which is not quantified when using a single series of μFE-models. By using multiple density thresholds to develop two series of μFE-models that include tissue of different densities, the aim of this study was to investigate the contribution of lower-mineralized tissue to the stiffness of fractured distal radii during the first twelve weeks of healing. Additionally, we evaluated bone mineral density as well as the contribution of lower-mineralized tissue to bone volume fraction using a similar dual-threshold approach to get more insights into the formation and mineralization of lower-mineralized tissue during healing.

2. Material and methods

2.1. Study design and participants

Data for this study were pooled data obtained from a single-blind randomized controlled trial (RCT) evaluating the effect of calcium and vitamin D supplementation on the healing of distal radius fractures. For that RCT, women aged 50 years and older with a stable distal radius fracture immobilized with a cast were included. Exclusion criteria were: 1) surgical fracture treatment or (bone) surgery of the current fracture side in medical history; 2) active or suspected infection in the past three months; 3) malignancy or pathological fracture in the past twelve months; 4) neuromuscular or neurosensory condition; 5) known systemic or metabolic bone disorder that leads to progressive bone deterioration; 6) active inflammatory disease in the past year; 7) use of oral glucocorticoids in the past twelve months; 8) allergy to any component of the calcium and vitamin D supplements prescribed as part of the RCT; and 9) severe concurrent joint involvement. Women provided written informed consent before study participation. The study protocol was approved by the institutional Medical Ethics Committee (METC registration number NL46035.072.13) and submitted to the Dutch Trial Register.

2.2. HR-pQCT imaging

2.2.1. Scan acquisition and grading

HR-pQCT (XtremeCT II, Scanco Medical, Switzerland) scans of the fractured distal radius were obtained using default clinical settings [23]. Scans were taken at four visits: the first, baseline (BL) scan at 1–2 weeks after fracture and three follow-up scans at 3–4, 6–8, and 12 weeks post-fracture. The scan protocol was used as in previous HR-pQCT research on distal radius fractures [19]. Using this protocol, a 20.4-mm region (two consecutive stacks) was scanned at each visit, which started 3 mm proximally from the reference line positioned at the proximal edge of the lunate bone. The lunate bone was used for the positioning of the reference line because the standard reference line position at the articular surface of the distal radius may not be possible in case of a distal radius fracture. The acquisition of two stacks was chosen to capture the entire fracture. During scan acquisition, the wrist was immobilized with a fiber-glass cast and additionally placed in a standard motion restraining holder. The cast was retained after cast removal and re-used for the remaining scans. Nevertheless, eleven patients wore a Plaster-of-Paris cast during one or more scan acquisitions due to the planning of their visits at the outpatient clinic, and one of them wore a brace during scan acquisition at another visit. Another patient wore a brace at every visit, and one patient wore no cast at one visit. A scan was repeated once if motion artefacts were observed on the preview slice. Scan time and effective radiation dose were approximately 4 min and 10 μSv per scan, respectively. The scans were reconstructed with an isotropic voxel size of 61 μm. After reconstruction, the quality of each stack of the scans was graded according to the five-point grading system described by Pialat et al. [24]. Scans with a grade 4 or 5 in one or both stacks were excluded from analysis; *i.e.*, only scans with grade 1–3 in both stacks were analyzed.

2.2.2. Scan analysis

From the scans with a grade 1–3 in both stacks, the distal radius was contoured and subsequently analyzed. Contouring was performed using an automatic contouring algorithm with manual adjustment in case of visual deviations from the outer bone margins [25]. Thereafter, stiffness in compression (S), bone volume fraction (BV/TV), and bone mineral density (BMD) were determined from the entire contoured bone region on the scans. Scan registration was not performed as three-dimensional registration algorithms did not yield correct alignment results for severe

fractures with substantial shape changes during healing [26,27]. BMD was quantified using standard evaluation methods [23]. *S* and BV/TV were quantified twice, once including only higher-mineralized tissue and once including higher- and lower-mineralized tissue. Higher-mineralized tissue was defined as having a density of >320 mg HA/cm^3, equaling the threshold that is standardly used in HR-pQCT analyses for trabecular bone [23]. Lower-mineralized tissue was defined as having a density of 200–320 mg HA/cm^3 based on the range of density thresholds previously used in an HR-pQCT study on local bone remodeling during distal radius fracture healing [17]. The thresholds of 200 mg HA/cm^3 and 320 mg HA/cm^3 correspond to approximately 17 % and 27 %, respectively of the assumed maximum density of fully mineralized bone by the manufacturer of the scanner (1200 mg HA/cm^3) [23].

To compute the two values of *S*, two series of linear micro-finite element (μFE-) models were used (Fig. 1). Both models were generated by conversion of the bone voxels of the HR-pQCT scans to equally-sized μFE-elements. For one series of models (M_{single}), the bone voxels were obtained by segmentation of the distal radii from the scans using a threshold of 320 mg HA/cm^3. For the second series of models (M_{dual}), a dual-threshold segmentation approach was adopted. Using this approach, the distal radii were segmented from the scans using a threshold of 200 mg HA/cm^3, followed by erosion of the resulting binarized image by one voxel to remove partial volume effect voxels. The result was then combined with the single-threshold model M_{single} to obtain the dual-threshold model M_{dual} that differentiates between higher-mineralized (>320 mg HA/cm^3) and lower-mineralized (200–320 mg HA/cm^3) tissue. The μFE-elements of both models were assigned a Poisson's Ratio of 0.3 and a Young's Modulus of 10 GPa for the higher-mineralized tissue, conform standard protocol [23]. For the lower-mineralized tissue, we used three different Young's Moduli in three separate analyses. Based on our defined density range for the lower-mineralized tissue (200–320 mg HA/cm^3) and higher-mineralized tissue (320–1200 mg HA/cm^3), we estimated a three times lower average density for the lower-mineralized tissue than for the higher-mineralized tissue. By assuming a linear relationship between the density and Young's Modulus for woven bone [28], we estimated also a three-times lower Young's Modulus (*i.e.* 3 GPa). Based on that estimate, we used a Young's Modulus of 1 GPa and 5 GPa for the lower-mineralized tissue. We additionally used a value of 10 GPa for this tissue (*i.e.* equal to the Modulus of the higher-mineralized tissue). An axial compression to 1 % strain was then applied to the μFE-models to calculate *S* as the reaction force over the applied displacement: S_{single} from M_{single} and S_{dual1}, S_{dual5}, and S_{dual10} from M_{dual} using a Young's Modulus of 1, 5, or 10 GPa, respectively for the lower-mineralized tissue. To compute the two values of BV/TV, the bone was segmented from the scans using a density threshold of either 200 mg HA/cm^3 (BV/TV$_{200}$) or 320 mg HA/cm^3 (BV/TV$_{320}$). For all parameters, all other settings regarding the segmentation and preprocessing of the scans were kept as default for second-generation HR-pQCT; *i.e.* Gaussian filtering with $\sigma = 0.8$ and support = 1 voxel [23]. The contribution of the lower-mineralized tissue to *S* and BV/TV was defined as the ratio of two stiffness parameters (S_{dual}/S_{single}) and the ratio of the two BV/TV parameters (simplifying to BV$_{200}$/BV$_{320}$), respectively.

2.3. Statistical analysis

Data were analyzed after pooling the data of the study groups. Results per study group are in Appendix 1. To quantify the differences in the absolute values and ratio of *S* and BV/TV over time, linear mixed-effect models (LMMs) were used. In the models, time post-fracture was included as fixed effect, the individual patients as random intercept, and age as covariate. The values from the LMMs at each timepoint were expressed as estimated marginal means (EMMs) with 95 %-confidence intervals (95 %-CI). The significance of the differences in the EMMs between timepoints was determined on a pairwise-basis. Multiple comparisons were adjusted using Bonferroni, and the significance level was set at $\alpha = 0.05$. The statistical analyses were performed in SPSS (SPSS 26.0, IBM Corp., Armonk, NY, USA) and R (R Foundation for Statistical Computing, Version R-3.6.2 for Windows, Vienna, Austria).

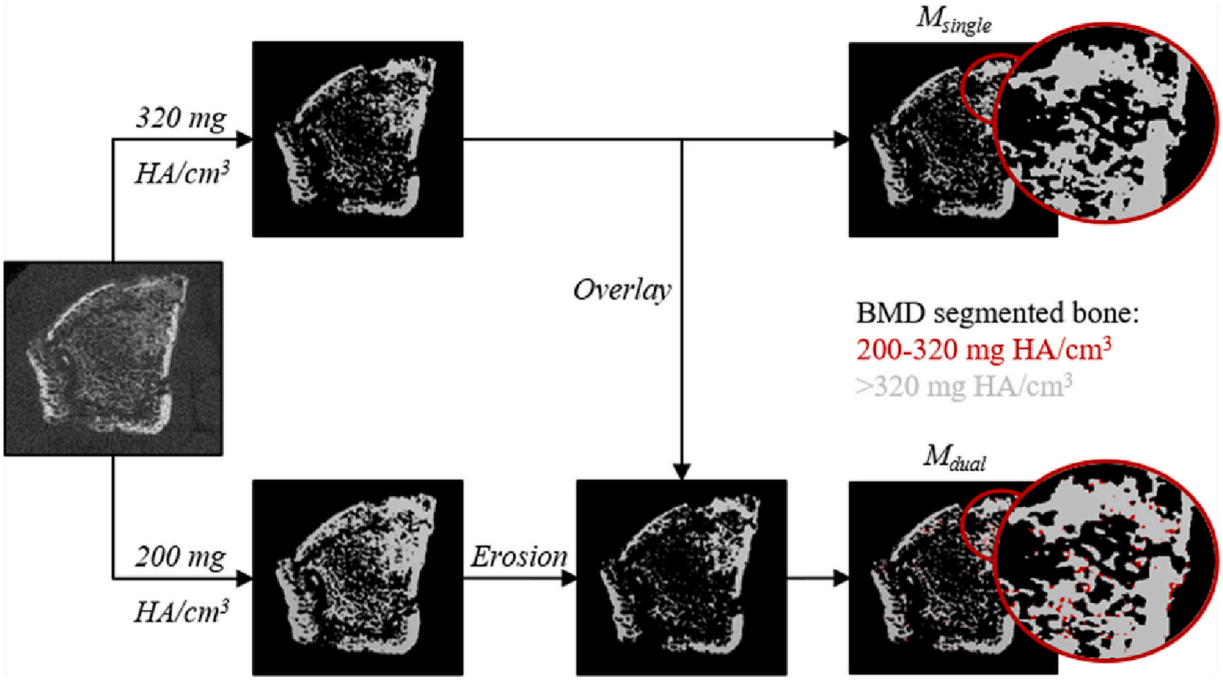

Fig. 1. Overview of the two series of micro-finite element (μFE-) models generated from the HR-pQCT scans of fractured distal radii during healing. One series (top) was based on segmentation of the distal radius using a threshold of 320 mg HA/cm^3 and thereby included only higher-mineralized tissue (>320 mg HA/cm^3). The other series (bottom) was based on a dual-threshold segmentation approach, for which the distal radius was segmented using a threshold of 200 mg HA/cm^3, followed by erosion by one voxel and then combination with the single-threshold model. This model thereby differentiated between higher-mineralized (>320 mg HA/cm^3) and lower-mineralized (200–320 mg HA/cm^3) tissue.

3. Results

3.1. Patient characteristics

In total, 52 women with a conservatively-treated distal radius fracture were included in this study of whom 48 completed the visits until 12 weeks post-fracture (Fig. 2). One of the 48 women missed the study visit at 6–8 weeks, so a total of 191 HR-pQCT scans was available. Of these scans, 29 were excluded from quantitative analysis: all scans of three women (*i.e.* 12 scans) due to insufficient quality of one or both stacks of three out of the four obtained HR-pQCT scans and 17 scans of 11 other women due to insufficient quality of one or both stacks of those scans. Resultingly, 162 scans of 45 women were quantitatively analyzed: 43, 38, 39, and 42 scans per visit. Characteristics of this cohort are listed in Table 1. The duration of cast treatment was 5.0 (interquartile range: 1.1) weeks in the 45 women. It ranged between 3.6 and 6.4 weeks for all but one who had cast treatment for only 1.7 weeks and wore a brace for an additional 2.6 weeks due to heavy swelling and pain while wearing the cast.

Table 1
Baseline characteristics of the women with analyzed HR-pQCT data ($N = 45$).

Age [year]	64.9 (13.9)
Calcium intake [mg/day][a]	755 (425)
<1000	28 (66.7)
<1200	39 (92.9)
25(OH)D level [nmol/L]	56 (48)
<50	17 (37.8)
<75	30 (66.7)
PTH [pmol/L]	5.1 (3.5)
aBMD *T*-score [−][b]	
Femoral neck	−2.0 (1.0)
Total hip	−1.4 (1.2)
Lumbar spine	−2.0 (1.3)
Osteoporosis [yes]	17 (37.8)

Values are reported as median (interquartile range) or number (%).
25(OH)D, 25-hydroxy-vitamin D. PTH, parathyroid hormone. aBMD, areal bone mineral density from dual-energy X-ray absorptiometry.
[a] n = 42.
[b] n = 43.

3.2. S, BV/TV, and BMD during fracture healing

The changes during healing in S are visualized in Fig. 3. S_{single} and S_{dual5} gradually increased over time to become significantly higher than BL at the 12-week visit (both $p < 0.0001$; Fig. 3a). At the 12-week visit, they were also significantly higher than at the visits at 3–4 weeks (both $p < 0.0001$) and 6–8 weeks (S_{single}: $p < 0.0001$; S_{dual5}: $p = 0.0001$) post-fracture. Similar changes were found when a lower or higher Young's Modulus was used for the lower-mineralized tissue in the dual-threshold μFE-models (Fig. 3b). S_{dual1} was significantly higher than BL at 12 weeks post-fracture ($p < 0.0001$). At this timepoint, it was also significantly higher than at 3–4 weeks ($p < 0.0001$) and 6–8 weeks ($p = 0.0001$) post-fracture. S_{dual10} was significantly higher than BL at 6–8 weeks ($p = 0.0384$) and 12 weeks ($p < 0.0001$) post-fracture. At 12 weeks, it was additionally significantly higher than at 3–4 weeks ($p < 0.0001$) and 6–8 weeks ($p = 0.0002$). The interindividual variation was considerable for all parameters of S.

The changes during healing in BV/TV and BMD followed different courses (Fig. 4). BV/TV_{320} and BV/TV_{200} significantly increased compared to BL at 3–4 weeks post-fracture ($p = 0.0403$ and $p = 0.0003$, respectively; Fig. 4a). They remained significantly higher than BL at 6–8 weeks post-fracture (BV/TV_{320}: $p = 0.0043$; BV/TV_{200}: $p = 0.0002$) and at 12 weeks post-fracture (BV/TV_{320}: $p = 0.0022$; BV/TV_{200}: $p = 0.0443$). BMD also significantly increased compared to BL at 3–4 weeks post-fracture ($p = 0.0108$; Fig. 4b). It returned to BL-values at 6–8 and 12 weeks post-fracture. At 12 weeks post-fracture, BMD was significantly lower than at 3–4 weeks post-fracture ($p = 0.0061$). Similar as for the S parameters, the interindividual variation was considerable for the

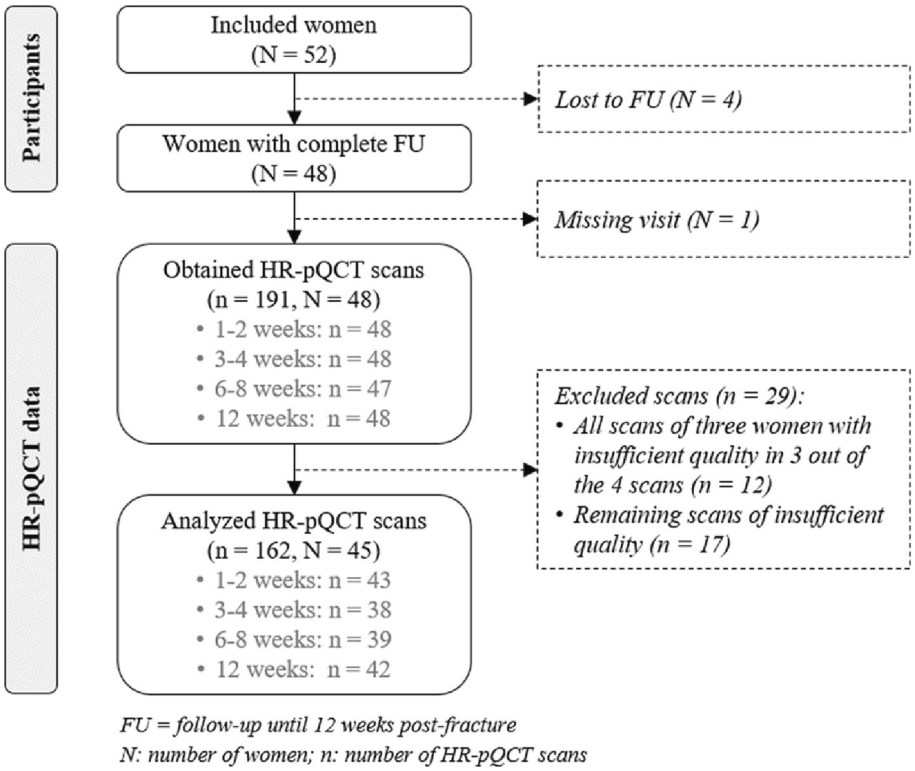

Fig. 2. Study participants and HR-pQCT data analyzed for this study.

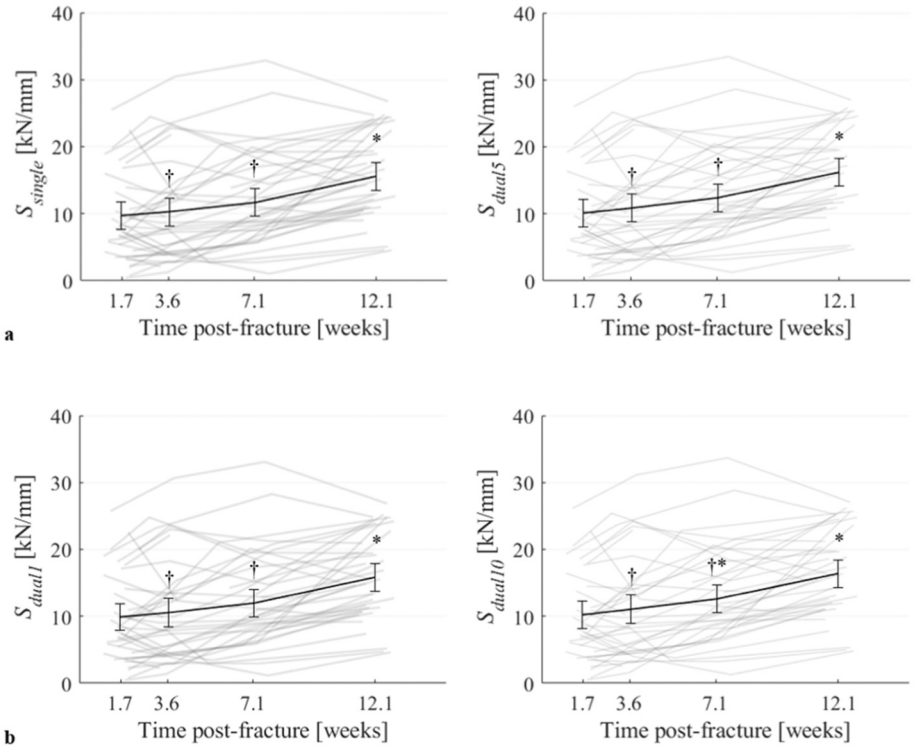

Fig. 3. Changes during fracture healing in stiffness a) from the single-threshold μFE-model (left) and the dual-threshold μFE-model with a Young's Modulus of 5 GPa for the lower-mineralized tissue (right); and b) from the dual-threshold μFE-models with a Young's Modulus of 1 GPa (left) and 10 GPa (right) for the lower-mineralized tissue. The black lines denote estimated marginal means with 95 %-confidence intervals. * and † denote a significant difference from the first and last visit, respectively ($p < 0.05$).

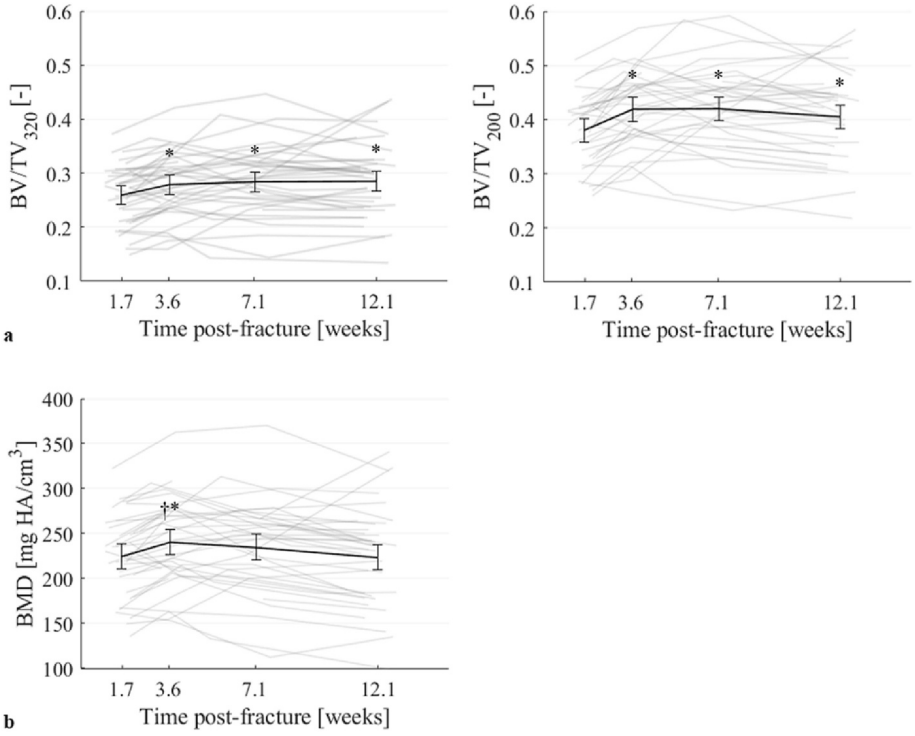

Fig. 4. Changes during fracture healing in a) bone volume fraction based on a density threshold for segmentation of 320 mg HA/cm^3 (left) and of 200 mg HA/cm^3 (right); and in b) bone mineral density. The black lines denote estimated marginal means with 95 %-confidence intervals. * and † denote a significant difference from the first and last visit, respectively ($p < 0.05$).

two BV/TV parameters and BMD.

3.3. Contribution of lower-mineralized tissue during healing

The changes in the ratio S_{dual5}/S_{single} showed a different course during healing than the changes in S (Fig. 5). The ratio significantly increased compared to BL at 3–4 weeks post-fracture ($p = 0.0010$), remained significantly higher than BL at 6–8 weeks post-fracture ($p < 0.0001$), and then decreased to BL-values at the 12-week visit (Fig. 5a). At this timepoint, the ratio was significantly lower than at 3–4 weeks

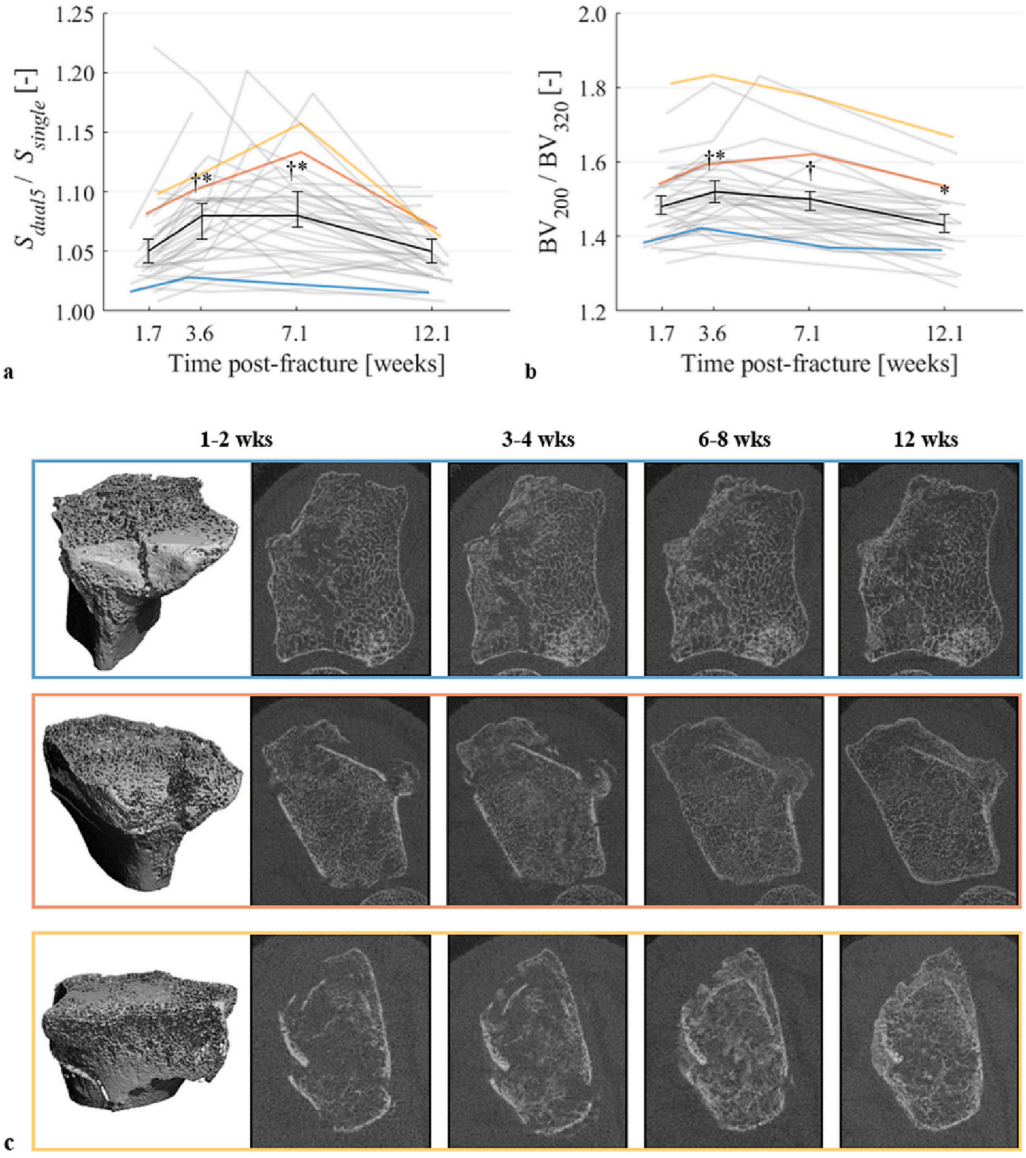

Fig. 5. Changes during fracture healing in the contribution of lower-mineralized tissue to a) stiffness represented by the ratio of stiffness from the dual-threshold μFE-model with a Young's Modulus of 5 GPa for the lower-mineralized tissue and the single-threshold μFE-model; and b) bone volume fraction represented by the ratio of bone volume fraction obtained using a segmentation threshold of 200 mg HA/cm^3 and of 320 mg HA/cm^3. The black lines denote estimated marginal means with 95 %-confidence intervals. * and † denote a significant difference from the first and last visit, respectively ($p < 0.05$). c) Comparable HR-pQCT slices during healing of three fractures with corresponding contribution of lower-mineralized tissue to stiffness and bone volume fraction. For visualization purposes, the scans were three-dimensionally registered based on their largest common height [27].

and 6–8 weeks (both $p < 0.0001$) post-fracture. The EMMs ranged between 1.05 (95 %-CI: 1.04–1.06) at 1–2 and 12 weeks post-fracture and 1.08 (1.07–1.10) at 6–8 weeks; *i.e.* the contribution of lower-mineralized tissue to *S* was 5–8 % at the group level. At the individual level, the ratio ranged between 1.01 and 1.22 (*i.e.* a contribution of 1–22 %). Similar results were found when a lower or higher Young's Modulus was used for the lower-mineralized tissue in the dual-threshold μFE-model (Fig. 6). The EMMs for the ratio ranged between 1.02 (1.01–1.03) at 12 weeks and 1.04 (1.03–1.04) at 3–4 and 6–8 weeks when a Young's Modulus of 1 GPa (S_{dual1}/S_{single}) was used and between 1.06 (1.05–1.08) at 12 weeks and 1.11 (1.09–1.12) at 6–8 weeks when a Young's Modulus of 10 GPa (S_{dual10}/S_{single}) was used. At the individual level, the ratio ranged between 1.00 and 1.12 (S_{dual1}/S_{single}) and 1.01–1.32 (S_{dual10}/S_{single}).

A similar course was found for the changes in the ratio BV_{200}/BV_{320} during healing (Fig. 5b). It significantly increased compared to BL at 3–4 weeks post-fracture ($p = 0.0023$) and subsequently decreased to become significantly lower than BL at 12 weeks post-fracture ($p < 0.0001$). At 12 weeks, the ratio was significantly lower than at 3–4 and 6–8 weeks post-fracture (both $p < 0.0001$). The EMMs ranged between 1.43 (1.41–1.46) and 1.52 (1.49–1.55). Fig. 5c shows three examples of fractures of visually varying severity and course and corresponding

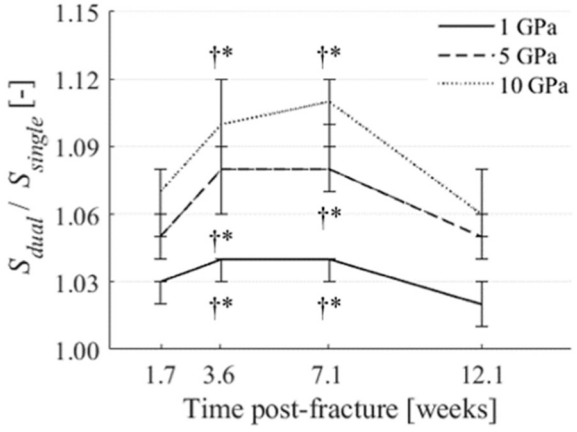

Fig. 6. Changes during fracture healing in the contribution of lower-mineralized tissue to stiffness represented by the ratio of stiffness from a dual-threshold μFE-model with a Young's Modulus of 1, 5, or 10 GPa for the lower-mineralized tissue and the single-threshold μFE-model. The lines denote estimated marginal means with 95 %-confidence intervals. * and † denote a significant difference from the first and last visit, respectively ($p < 0.05$).

contribution of lower-mineralized tissue to *S* and BV/TV during healing.

4. Discussion

The aim of this study was to investigate the contribution of lower-mineralized tissue to the stiffness of fractured distal radii derived from HR-pQCT during the first twelve weeks of healing by using multiple density thresholds to develop two series of μFE-models that include tissue of different mineralization densities. Additionally, we quantified bone mineral density and the contribution of lower-mineralized tissue to bone volume fraction to evaluate the formation and mineralization of lower-mineralized tissue during healing. While the stiffness of the distal radius fractures significantly increased compared to BL at the 12-week visit, the contribution of lower-mineralized tissue to the stiffness increased significantly compared to BL at 3–4 weeks and 6–8 weeks post-fracture. The course and statistical significance of the longitudinal changes were independent of the Young's Modulus used for the lower-mineralized tissue in the dual-threshold μFE-model (between 1 and 10 GPa). When using a Young's Modulus of 5 GPa for the lower-mineralized tissue, the magnitude of the contribution of the lower-mineralized tissue to stiffness was 5–8 % at the group level and 1–22 % at the individual level. The contribution of lower-mineralized tissue to bone volume fraction had a similar course during healing but larger magnitude. Bone mineral density significantly increased compared to BL at 3–4 weeks and returned to BL-values thereafter.

Combining stiffness results that are obtained using different density thresholds for segmentation enables quantification of the contribution of lower-mineralized tissue to the stiffness of fractured distal radii during healing. The contribution of this tissue to stiffness significantly increased compared to BL at 3–4 and 6–8 weeks post-fracture. At 3–4 weeks post-fracture, bone volume fraction and bone mineral density were also significantly higher than at BL, together with a significantly increased contribution of lower-mineralized tissue to bone volume fraction. These changes suggest the formation of lower-mineralized tissue early during healing. The timing of these changes co-occurs with visual changes of trabecular structures around the fracture region reported from 3 to 4 weeks post-fracture [15] and is consistent with the findings in a histological study on human specimens of distal radius fractures, where (woven) bone formation was observed between 2 and 4 weeks post-fracture but not in the first week after fracture [29]. At later timepoints, the contribution of lower-mineralized tissue to bone volume fraction decreased. This suggests remodeling of the lower-mineralized tissue towards higher-mineralized bone. Together, the changes we found during healing support the general knowledge on the early phases of fracture healing; *i.e.* formation and concomitant and subsequent remodeling of woven bone [20–22].

The changes in the contribution of lower-mineralized tissue to stiffness preceded the changes in stiffness, which significantly increased compared to BL at 6–8 or 12 weeks post-fracture depending on the Young's Modulus for the lower-mineralized tissue. Together with the changes in the contribution of lower-mineralized tissue to bone volume fraction during healing, it suggests that predominantly mature bone, formed by remodeling of early lower-mineralized bone, contributes to the recovery of biomechanical strength after fracture. Stiffness from μFE-analysis may continue to increase until months after cast removal [16,18]. Simultaneously, Dutch guidelines prescribe cast treatment after a distal radius fracture for only 3–5 weeks [5]. At that time, we found limited signs of biomechanical fracture recovery as assessed by the stiffness from μFE-analysis but a significant increase compared to BL in the contribution of lower-mineralized tissue to this stiffness. Possibly, the lower-mineralized tissue provides sufficient fracture stabilization for cast removal, which is captured by changes in the contribution of lower-mineralized tissue to stiffness but not by changes in stiffness. That is, quantification of the contribution of lower-mineralized tissue to stiffness provides quantitative information about the early phases of fracture healing, which may be clinically most relevant. It additionally gives a more complete impression of strength recovery post-fracture than the evaluation of stiffness using a single series of μFE-models.

In contrast to the course and timing of the contribution of lower-mineralized tissue to stiffness during healing, the magnitude of this contribution is likely less physiologically accurate due to the used methodology. For example, the erosion step used to obtain the dual-threshold μFE-models might have led to an underestimation of the magnitude due to the potential exclusion of lower-mineralized voxels in the μFE-models that were not the effect of partial volume effects but true voxels of lower-mineralized tissue. Additionally, the material properties of lower-mineralized tissue are not fully known, for which reason we used a range of Young's Moduli (1–10 GPa) in our dual-threshold μFE-models. The upper value of this range (10 GPa) equals the value often used for mature bone in μFE-models from HR-pQCT data and can thus be considered as the theoretical maximum. This value likely overestimates the material properties of the lower-mineralized tissue and thereby the contribution of this tissue to stiffness. It is unknown whether the lower value of the chosen range (1 GPa) would be the physiological minimum. The material properties of the lower-mineralized tissue may also not be constant between regions and during the fracture healing process [30]. Besides that, the estimates of stiffness may not be fully accurate. While μFE-models similar to our single-threshold model accurately estimate failure load at the distal radius [31], μFE-analysis can considerably overestimate the stiffness of fractured bones depending on the type of fracture [32]. More detailed μFE-models (*e.g.* gray-value based with density-dependent material properties [33,34]) could possibly provide more accurate estimates, but the sole contribution of lower-mineralized tissue to stiffness cannot be quantified using a single series of FE-models, independent of the amount of detail. We did not experimentally validate our findings on the contribution of lower-mineralized tissue to stiffness. Such validation would also be challenging if not impossible because lower-mineralized tissue would not be easily separable from the rest of the bone tissue, and mechanical loads cannot be applied to solely this tissue. Nevertheless, our results suggest that the magnitude of the contribution of lower-mineralized tissue to stiffness as assessed by HR-pQCT is minor, and that the course and timing of the contribution during healing may be clinically relevant.

There was large inter- and intraindividual variability in the evaluated parameters, which could be associated with fracture type and patient characteristics. Fracture pattern and severity varied highly among the participants and might influence the extent to which lower-mineralized tissue is formed during healing and thereby the extent to which it contributes to the healing process. Furthermore, fracture dislocations during healing may cause differences in the scanned and analyzed bone region over time, which could have contributed to the large and abrupt longitudinal changes observed at the individual level. Similarly, patient characteristics, such as age and bone quality, might have contributed to the interindividual variation. Age and post-menopausal osteoporosis may influence biological and mechanical factors involved in multiple phases of fracture healing [35–37], although evidence mainly comes from animal studies and is not convincing in clinical studies [36,37]. Additionally, in osteoporotic bone with less and lower-mineralized bone tissue, the contribution of lower-mineralized tissue might be relatively larger than in healthy bone, possibly further influenced by the phenotype of osteoporotic bone microarchitecture [38]. Further research into the role of lower-mineralized tissue in fracture healing may include fracture pattern and severity and patient characteristics to improve our understanding of the fracture healing process in elderly and the effects of fracture type.

Another important aspect regarding the inter- and intraindividual variability is the reproducibility of our methodology. Repositioning errors between visits and motion artefacts might have contributed to the differences between participants and within participants between timepoints. Motion artefacts are partly inherent to the use of HR-pQCT and μFE-analysis: the relatively long scan time of HR-pQCT increases the risk of patient movement, and the large detail of both techniques

increases the potential effects of this movement on the quantified parameters. Scanning multiple stacks furthermore introduces a specific type of motion artefacts, stack shifts. Such shifts may potentially influence HR-pQCT parameters, but this influence is unknown. In a pilot study, we evaluated the effects of correcting stack shifts using an in-house developed stack registration algorithm on the stiffness from μFE-analysis at the contralateral, non-fractured distal radius of the participants of the current study. Using this algorithm, a two-layer overlap was artificially generated between the two stacks of an HR-pQCT scan, followed by three-dimensional rigid registration to compute an in-plane translation that was then applied to one of two stacks to reduce the stack shift. Preliminary analyses on 76 contralateral HR-pQCT scans showed that the median absolute percentage change in stiffness after stack shift correction was 0.94 % (interquartile range 1.8 %), and it was $\leq$1 % in 40 out of the 76 scans (52.6 %; data not shown). Further study is however warranted to evaluate the need and the effects of a stack shift correction. Nevertheless, the fracture-, patient-, and reproducibility-related factors challenge the interpretation of results obtained with our methodology at the individual level as changes in the parameters during healing may not be solely the result of metabolic changes but also of these factors.

In contrast, at the group level in clinical studies, where a combination of objective and subjective outcome measures is recommended to assess fracture healing [39], our methodology could be used to obtain quantitative and objective data on early changes during fracture healing based on detailed microarchitectural information of a fracture. The contribution of lower-mineralized tissue to stiffness could for example be a valuable measure. It requires however multiple μFE-analyses, which is computationally expensive. The contribution of lower-mineralized tissue to bone volume fraction is easier to compute and computationally less expensive and had a similar course during fracture healing. The magnitude was however considerably higher, which may result among others from differences in computation (*e.g.* an erosion step was used in the generation of the dual-threshold μFE-models but not in the computation of bone volume fraction) and relative contribution of the voxels (*e.g.* included voxels may not all have contributed to a measurable extent to stiffness due to for example their location outside the fracture region, while all included voxels add to bone volume fraction). Nevertheless, the contribution of lower-mineralized tissue to bone volume fraction could be an alternative measure for the contribution to stiffness in the quantification of early changes during fracture healing.

Our study has several limitations. First, we used a scan protocol in which scan length and region were fixed for each participant, independent of the size and precise location of the fracture. Consequently, the fracture was not entirely captured in all participants. Furthermore, this protocol has likely resulted in a variable fracture volume relative to the scanned volume among participants, thereby potentially underestimating the contribution of lower-mineralized tissue to the fracture healing in participants with a relatively small fracture. Future studies may therefore consider the use of a scan protocol with variable scan length and region and evaluation of subregions within the scanned bone that contain the fracture. Second, we based the density threshold for the lower-mineralized tissue on the thresholds used in a previous HR-pQCT study on distal radius fracture healing, in which the participants were younger than the participants in our study [17]. However, as the degree of mineralization of lower-mineralized tissue may not depend on age, we used the same threshold as in that study for uniformity. Furthermore, a lower threshold could potentially lead to a more noisy segmentation result and to the inclusion of tissue that likely does not add to the stabilization of a fracture. Third, the scan region may have differed within participants between timepoints due to repositioning errors and the use of the lunate bone to determine the scan region which position with respect to the distal radius is not fixed. We did not align the scans to correct these potential differences in scan region because three-dimensional registration algorithms did not yield accurate results for severe fractures with substantial shape changes during healing [26,27]. A previously explored registration algorithm based on aligning fracture fragments was not evaluated [40]. Fourth, we did not correct for differences in the cast worn during scan acquisition nor for stack shifts. A cast can cause systematic errors in HR-pQCT parameters due to beam hardening, but correction is difficult as cast interference depends on among others cast type and thickness [41,42]. Stack shifts could potentially influence HR-pQCT parameters, but the effects are unknown. As mentioned previously, preliminary analyses on contralateral HR-pQCT scans of the participants of the current study showed that the median absolute percentage change in stiffness after stack shift correction was <1 % (data not shown), but further evaluation is required to study the need and the effects of a stack shift correction. Fifth, the automatically obtained contours of the fractured distal radii required considerable manual adjustment, which is subjective, especially in largely compressed fractures and due to lower-mineralized tissue formation. However, all adjustments were performed by the same investigator (MB), and μFE-parameters are little influenced by the periosteal contouring as long as all bone is included in the contoured region. Recently, an automatic contouring algorithm has been developed for fractured distal radii, but this algorithm was not available for use in our center [43]. Finally, as mentioned previously, the computed stiffness and contribution of lower-mineralized tissue to stiffness are likely not fully physiologically accurate [32], and therefore the magnitude of the contribution of the lower-mineralized tissue to stiffness may not be fully accurate. Nevertheless, the course and timing of the contribution agree with general knowledge on fracture healing, and quantification of early changes may have clinical relevance.

To conclude, combining stiffness results from two series of μFE-models obtained using single- and dual-threshold segmentation enables quantification of the contribution of lower-mineralized tissue to fracture stiffness. The contribution of this tissue to the stiffness of conservatively-treated distal radius fractures is minor but changes significantly early during healing and around the time of cast removal. Together with changes in the contribution of lower-mineralized tissue to bone volume fraction, it may reflect the formation of woven bone and its subsequent and concomitant remodeling to mature bone. While the magnitude of the contribution to stiffness during healing may physiologically not be fully accurate, the course and timing of this contribution could be clinically relevant. Quantification of the contribution of lower-mineralized tissue to stiffness additionally gives a more complete impression of strength recovery post-fracture than the evaluation of stiffness using a single series of μFE-models alone.

Funding

This study is funded by the Weijerhorst Foundation and by the Science and Innovation Fund of VieCuri Medical Center, Venlo, The Netherlands.

CRediT authorship contribution statement

Melissa S.A.M. Bevers: Writing – review & editing, Writing – original draft, Visualization, Software, Methodology, Investigation, Formal analysis, Data curation, Conceptualization. **Frans L. Heyer:** Writing – review & editing, Writing – original draft, Project administration, Methodology, Investigation, Data curation, Conceptualization. **Caroline E. Wyers:** Writing – review & editing, Writing – original draft, Supervision, Project administration, Methodology, Investigation, Conceptualization. **Bert van Rietbergen:** Writing – review & editing, Writing – original draft, Supervision, Software, Methodology, Conceptualization. **Piet P.M.M. Geusens:** Writing – review & editing, Writing – original draft, Supervision, Methodology, Conceptualization. **Heinrich M.J. Janzing:** Writing – review & editing, Resources, Conceptualization. **Okke Lambers Heerspink:** Writing – review & editing, Resources, Conceptualization. **Martijn Poeze:** Writing – review & editing, Conceptualization. **Joop P. van den Bergh:** Writing – review & editing,

Writing – original draft, Supervision, Resources, Project administration, Methodology, Funding acquisition, Conceptualization.

Declaration of competing interest

B. van Rietbergen is a consultant for Scanco Medical AG. J.P. van den Bergh is a consultant for Porous GmbH. All other authors declare that they have no conflicts of interest.

Data availability

The authors do not have permission to share data.

Acknowledgements

We thank Sania Moharir, BSc for her help in studying the effects of stack shifts on μFE-analyses as part of her Master graduation project.

Appendix A. Supplementary data

Supplementary data to this article can be found online at https://doi.org/10.1016/j.bone.2023.116859.

References

[1] J.A. Baron, M. Karagas, J. Barrett, W. Kniffin, D. Malenka, M. Mayor, R.B. Keller, Basic epidemiology of fractures of the upper and lower limb among Americans over 65 years of age, Epidemiology 7 (6) (1996) 612–618.
[2] J.W. Karl, P.R. Olson, M.P. Rosenwasser, The epidemiology of upper extremity fractures in the United States, 2009, J. Orthop. Trauma 29 (8) (2015) e242–e244.
[3] K.W. Nellans, E. Kowalski, K.C. Chung, The epidemiology of distal radius fractures, Hand Clin. 28 (2) (2012) 113–125.
[4] K.C. Chung, M.J. Shauver, J.D. Birkmeyer, Trends in the United States in the treatment of distal radial fractures in the elderly, J. Bone Joint Surg. Am. 91 (8) (2009) 1868.
[5] NVVH, "Distale radiusfracturen – Duur immobilisatie bij distale radiusfracturen". Richtlijnendatabase. https://richtlijnendatabase.nl/richtlijn/distale_radiusfracturen/duur_immobilisatie_bij_distale_radiusfracturen.html, 2021. Accessed 1 April 2023 [Dutch].
[6] A. Bentohami, E.A.K. van Delft, J. Vermeulen, N.L. Sosef, N. de Korte, T.S. Bijlsma, J.C. Goslings, N.W.L. Schep, Non-or minimally displaced distal radial fractures in adult patients: three weeks versus five weeks of cast immobilization—a randomized controlled trial, J. Wrist Surg. 8 (01) (2019) 043–048.
[7] A. Christersson, S. Larsson, B. Östlund, B. Sandén, Radiographic results after plaster cast fixation for 10 days versus 1 month in reduced distal radius fractures: a prospective randomised study, J. Orthop. Surg. Res. 11 (1) (2016) 1–8.
[8] A. Christersson, S. Larsson, B. Sandén, Clinical outcome after plaster cast fixation for 10 days versus 1 month in reduced distal radius fractures: a prospective randomized study, Scand. J. Surg. 107 (1) (2018) 82–90.
[9] J. Goldhahn, D. Beaton, A. Ladd, J. Macdermid, A. Hoang-Kim, Recommendation for measuring clinical outcome in distal radius fractures: a core set of domains for standardized reporting in clinical practice and research, Arch. Orthop. Trauma Surg. 134 (2014) 197–205.
[10] L.A. Corrales, S. Morshed, M. Bhandari, T. Miclau III, Variability in the assessment of fracture-healing in orthopaedic trauma studies, J. Bone Joint Surg. Am. 90 (9) (2008) 1862.
[11] B.G. Dijkman, S. Sprague, E.H. Schemitsch, M. Bhandari, When is a fracture healed? Radiographic and clinical criteria revisited, J. Orthop. Trauma 24 (2010) S76–S80.
[12] S. Morshed, Current options for determining fracture union, Adv. Med. 2014 (2014).
[13] L.A. Lopas, H. Shen, N. Zhang, Y. Jang, V.L. Tawfik, S.B. Goodman, R.M. Natoli, Clinical assessments of fracture healing and basic science correlates: is there room for convergence? Curr. Osteoporosis Rep. (2022) 1–12.
[14] T.L. Mueller, A.J. Wirth, G.H. van Lenthe, J. Goldhahn, J. Schense, V. Jamieson, P. Messmer, D. Uebelhart, D. Weishaupt, M. Egermann, R. Müller, Mechanical stability in a human radius fracture treated with a novel tissue-engineered bone substitute: a non-invasive, longitudinal assessment using high-resolution pQCT in combination with finite element analysis, J. Tissue Eng. Regen. Med. 5 (5) (2011) 415–420.
[15] J.J. de Jong, P.C. Willems, J.J. Arts, S.G. Bours, P.R. Brink, T.A. van Geel, M. Poeze, P.P. Geusens, B. van Rietbergen, J.P. van den Bergh, Assessment of the healing process in distal radius fractures by high resolution peripheral quantitative computed tomography, Bone 64 (2014) 65–74.
[16] J.J. de Jong, F.L. Heyer, J.J. Arts, M. Poeze, A.P. Keszei, P.C. Willems, B. van Rietbergen, P.P. Geusens, J.P. van den Bergh, Fracture repair in the distal radius in postmenopausal women: a follow-up 2 years Postfracture using HRpQCT, J. Bone Miner. Res. 31 (5) (2016) 1114–1122.
[17] P.R. Atkins, K. Stock, N. Ohs, C.J. Collins, L. Horling, S. Benedikt, G. Degenhart, K. Lippuner, M. Blauth, P. Christen, R. Müller, Formation dominates resorption with increasing mineralized density and time postfracture in cortical but not trabecular bone: a longitudinal HRpQCT imaging study in the distal radius, JBMR Plus 5 (6) (2021), e10493.
[18] P. Spanswick, D. Whittier, C. Kwong, R. Korley, S. Boyd, P. Schneider, Restoration of stiffness during fracture healing at the distal radius, using HR-pQCT and finite element methods, J. Clin. Densitom. 24 (3) (2021) 422–432.
[19] F.L. Heyer, J.J. de Jong, P.C. Willems, J.J. Arts, S.G.P. Bours, S.M.J. van Kuijk, J.A. P. Bons, M. Poeze, P.P. Geusens, B. van Rietbergen, J.P. van den Bergh, The effect of bolus vitamin D3 supplementation on distal radius fracture healing: a randomized controlled trial using HR-pQCT, J. Bone Miner. Res. 36 (8) (2021) 1492–1501.
[20] R. Marsell, T.A. Einhorn, The biology of fracture healing, Injury 42 (2011) 551–555.
[21] O.H. Sandberg, P. Aspenberg, Inter-trabecular bone formation: a specific mechanism for healing of cancellous bone: a narrative review, Acta Orthop. 87 (5) (2016) 459–465.
[22] S. Inoue, H. Otsuka, J. Takito, M. Nakamura, Decisive differences in the bone repair processes of the metaphysis and diaphysis in young mice, Bone Rep. (2018) 81–88.
[23] D.E. Whittier, S.K. Boyd, A.J. Burghardt, J. Paccou, A. Ghasem-Zadeh, R. Chapurlat, K. Engelke, M.L. Bouxsein, Guidelines for the assessment of bone density and microarchitecture in vivo using high-resolution peripheral quantitative computed tomography, Osteoporos. Int. 31 (2020) 1607–1627.
[24] J.B. Pialat, A.J. Burghardt, M. Sode, T.M. Link, S. Majumdar, Visual grading of motion induced image degradation in high resolution peripheral computed tomography: impact of image quality on measures of bone density and micro-architecture, Bone 50 (1) (2012) 111–118.
[25] H.R. Buie, G.M. Campbell, R.J. Klinck, J.A. MacNeil, S.K. Boyd, Automatic segmentation of cortical and trabecular compartments based on a dual threshold technique for in vivo micro-CT bone analysis, Bone 41 (4) (2007) 505–515.
[26] R. Ellouz, R. Chapurlat, B. van Rietbergen, P. Christen, J.B. Pialat, S. Boutroy, Challenges in longitudinal measurements with HR-pQCT: evaluation of a 3D registration method to improve bone microarchitecture and strength measurement reproducibility, Bone 63 (2014) 147–157.
[27] B. van Rietbergen, E. Biver, T. Chevalley, K. Ito, R. Chapurlat, S. Ferrari, A novel HR-pQCT image registration approach reveals sex-specific changes in cortical bone retraction with aging, J. Bone Miner. Res. 36 (7) (2021) 1351–1363.
[28] J. Mora-Macías, P. García-Florencio, A. Pajares, P. Miranda, J. Domínguez, E. Reina-Romo, Elastic modulus of woven bone: correlation with evolution of porosity and x-ray greyscale, Ann. Biomed. Eng. 49 (2021) 180–190.
[29] P. Aspenberg, O. Sandberg, Distal radial fractures heal by direct woven bone formation, Acta Orthop. 84 (3) (2013) 297–300.
[30] I. Manjubala, Y. Liu, D.R. Epari, P. Roschger, H. Schell, P. Fratzl, G.N. Duda, Spatial and temporal variations of mechanical properties and mineral content of the external callus during bone healing, Bone 45 (2) (2009) 185–192.
[31] A.J. Arias-Moreno, H.S. Hosseini, M.S.A.M. Bevers, K. Ito, P. Zysset, B. van Rietbergen, Validation of distal radius failure load predictions by homogenized- and micro-finite element analyses based on second-generation high-resolution peripheral quantitative CT images, Osteoporos. Int. 30 (2019) 1433–1443.
[32] A.J. Arias-Moreno, K. Ito, B. van Rietbergen, Micro-finite element analysis will overestimate the compressive stiffness of fractured cancellous bone, J. Biomech. 49 (13) (2016) 2613–2618.
[33] S.J. Shefelbine, U. Simon, L. Claes, A. Gold, Y. Gabet, I. Bab, R. Müller, P. Augat, Prediction of fracture callus mechanical properties using micro-CT images and voxel-based finite element analysis, Bone 36 (3) (2005) 480–488.
[34] T. Suzuki, Y. Matsuura, T. Yamazaki, T. Akasaka, E. Ozone, Y. Matsuyama, M. Mukai, T. Ohara, H. Wakita, S. Taniguchi, S. Ohtori, Biomechanics of callus in the bone healing process, determined by specimen-specific finite element analysis, Bone 132 (2020), 115212.
[35] P. Augat, U. Simon, A. Liedert, L. Claes, Mechanics and mechano-biology of fracture healing in normal and osteoporotic bone, Osteoporos. Int. 16 (2005) S36–S43.
[36] P. Giannoudis, C. Tzioupis, T. Almalki, R. Buckley, Fracture healing in osteoporotic fractures: is it really different?: a basic science perspective, Injury 38 (1) (2007) S90–S99.
[37] E.A. Gorter, C.R. Reinders, P. Krijnen, N.M. Appelman-Dijkstra, I.B. Schipper, The effect of osteoporosis and its treatment on fracture healing a systematic review of animal and clinical studies, Bone Rep. 15 (2021), 101117.
[38] D.E. Whittier, E.J. Samelson, M.T. Hannan, L.A. Burt, D.A. Hanley, E. Biver, P. Szulc, E. Sornay-Rendu, B. Merle, R. Chapurlat, E. Lespessailles, A.K.O. Wong, D. Goltzman, S. Khosla, S. Ferrari, M.L. Bouxsein, D.P. Kiel, S.K. Boyd, Bone microarchitecture phenotypes identified in older adults are associated with different levels of osteoporotic fracture risk, J. Bone Miner. Res. 37 (3) (2022) 428–439.
[39] J. Goldhahn, F. Angst, B.R. Simmen, What counts: outcome assessment after distal radius fractures in aged patients, J. Orthop. Trauma 22 (2008) S126–S130.
[40] J.J. de Jong, P. Christen, R.M. Plett, R. Chapurlat, P.P. Geusens, J.P. van den Bergh, R. Müller, B. Van Rietbergen, Feasibility of rigid 3D image registration of high-resolution peripheral quantitative computed tomography images of healing distal radius fractures, PLoS One 12 (7) (2017), e0179413.
[41] J.J. de Jong, J.J. Arts, U. Meyer, P.C. Willems, P.P. Geusens, J.P. van den Bergh, B. van Rietbergen, Effect of a cast on short-term reproducibility and bone

parameters obtained from HR-pQCT measurements at the distal end of the radius, JBJS 98 (5) (2016) 356–362.
[42] D.E. Whittier, S.L. Manske, S.K. Boyd, P.S. Schneider, The correction of systematic error due to plaster and fiberglass casts on HR-pQCT bone parameters measured in vivo at the distal radius, J. Clin. Densitom. 22 (3) (2019) 401–408.
[43] N. Ohs, C.J. Collins, D.C. Tourolle, P.R. Atkins, B.J. Schroeder, M. Blauth, P. Christen, R. Müller, Automated segmentation of fractured distal radii by 3D geodesic active contouring of in vivo HR-pQCT images, Bone 147 (2021), 115930.